HAL
open science

Dynamics of Magnetic Islands driven by Ballooning Turbulence

N. Dubuit, O. Agullo, M. Muraglia, J. Frank, X. Garbet, P. Maget

To cite this version:

N. Dubuit, O. Agullo, M. Muraglia, J. Frank, X. Garbet, et al.. Dynamics of Magnetic Islands driven by Ballooning Turbulence. Physics of Plasmas, 2021, 28 (2), pp.022308. 10.1063/5.0021391 . hal-03030454v2

HAL Id: hal-03030454

https://hal.science/hal-03030454v2

Submitted on 22 Feb 2021

HAL is a multi-disciplinary open access archive for the deposit and dissemination of scientific research documents, whether they are published or not. The documents may come from teaching and research institutions in France or abroad, or from public or private research centers.

L'archive ouverte pluridisciplinaire **HAL**, est destinée au dépôt et à la diffusion de documents scientifiques de niveau recherche, publiés ou non, émanant des établissements d'enseignement et de recherche français ou étrangers, des laboratoires publics ou privés.

Dynamics of Magnetic Islands driven by Ballooning Turbulence

N. Dubuit,[1, a)] O. Agullo,[1] M. Muraglia,[1] J. Frank,[1] X. Garbet,[2] and P. Maget[2]
[1)] *Aix-Marseille Univ., CNRS, PIIM UMR 7345, Marseille, France*
[2)] *CEA, IRFM, F-13108 Saint-Paul-Lez-Durance, France*

Magnetic island generation by remote ballooning turbulence close to the plasma edge is investigated through flux-driven 3D Reduced-MHD simulations. The various coupling mechanisms are investigated : mono-helicity nonlinear coupling, multi-helicity nonlinear coupling and linear toroidal coupling. The dominant process depends on the imposed heat flux driving the turbulence. The remote drive happens in two successive phases corresponding to different coupling paths. While an island is remotely generated in both phases, it is dominated by different mode numbers, or harmonics, and therefore has a different shape. The size of the generated island is found to be proportional to the imposed heat flux, without threshold. The shape of the island in the saturated regime also depends on the imposed heat flux, with a more distorted shape at low power levels.

I. INTRODUCTION

In fusion devices, magnetic islands are commonly observed. Their growth, which is mainly driven by neoclassical effects, is important enough to strongly limit the thermal confinement of the plasma. Their presence can lead to a confinement degradation of more than 30% in large tokamaks[1] and can potentially induce disruptions. Such islands are called Neoclassical Tearing Modes (NTMs). Neoclassical effects however do not generate islands *ab initio* but only amplify large enough islands seeded by some other mechanisms. Although seed islands are often generated by large scale MHD events, sawteeth or edge localized modes, cases where their origin is not clear are also frequent[2–4]. In the last decade, the seeding of magnetic island by microturbulence has been investigated mainly in 2D context[5–11] or with more complete 3D descriptions[12,13] with a focus on the characterization of islands embedded and/or generated by in situ turbulence. However, it has been shown that remote turbulence can drive the growth of islands on low order magnetic surfaces[14]. This is important from an experimental point of view, since islands are commonly found in the plasma core, while turbulence is larger in the plasma edge ; however experimental work is usually focused on turbulence close to the island resonant surface[4,15,16]. From a fundamental point of view, remote generation has also the benefit to help separate the local flow dynamics of turbulence and that of the generated island[9,11,17]. Moreover, a 2D study has shown that turbulence-generated seed islands are potentially large enough to be amplified by bootstrap current and therefore give rise to a neoclassical tearing mode[18] and result in a loss of confinement or a disruption. Ballooning modes are the prototype of a class of instabilities that are ubiquitous the edge of tokamaks. They are characterized by higher growth rates than Ion Temperature Gradient (ITG) modes which dominate in the core. A natural question is, thus, to determine the mechanisms, and quantify their relative importance, from which ballooning modes could amplify and/or seed islands in the vicinity of core low order rational surface. Compared to the cylindrical previous work[14], here a flux driven ballooning turbulence is included. Various effects could alter the island seeding. First, the curvature terms include a linear poloidal coupling which naturally couples mode which resonate on different magnetic surfaces and thus, potentially, couple the edge dynamics to the core's one. Second, emphasizing that the nonlinear beating of modes has been already identified as part of key mechanisms on the seeding of islands, both in 2D and 3D cylindrical contexts and that this is linked to the nature (including their parities) of the mode structures, one should query this point in toroidal context. Indeed, ballooning modes contains intrinsic poloidal asymmetries which could weaken the coupling between modes. Third, helical magnetic perturbations are not anymore characterized by the existence of a invariant, the helical flux, along magnetic flux surfaces and overlap of islands can introduce stochasticity of the magnetic lines. Those lines can strongly connect distant radial zones and modify the overall dynamics. Thus, it is not obvious whether or not ballooning turbulence can amplify remotely magnetic islands and whether the mechanisms at play in previous works[6,14,19,20] remain dominant. Finally, the link between island size and the input power which alters the profiles and drives the turbulence, in flux driven context, has not been yet investigated.

The remainder of this paper is as follows. In section II the numerical model used for simulations is described. In section III, the seeding of magnetic islands by flux driven ballooning turbulence is investigated. The link between island dynamics, seed island size and input power is explored in section IV. Finally, the section V presents the conclusions of the paper.

II. NUMERICAL SETUP

We model the interaction of microturbulence and magnetic islands using a minimal 3D three-field reduced-MHD model, including toroidal curvature and flux driven

[a)] Electronic mail: nicolas.dubuit@univ-amu.fr

dynamics:

$$\partial_t \omega + [\phi, \omega] = -\kappa_1 G P + \nabla_\parallel J + \nu \Delta_\perp \omega \ , \tag{1}$$

$$\partial_t P + [\phi, P] = \kappa_2 G \phi + \kappa_2^P G P + \rho_\star^2 [\psi, J] + \chi \Delta_\perp P + S_P \ , \tag{2}$$

$$\partial_t \psi = \nabla_\parallel (\phi - P) + \eta j_\parallel \ , \tag{3}$$

where ϕ is the electrostatic potential, $\omega = \Delta_\perp \phi$ the vorticity, P the electron pressure, ψ the magnetic flux, $J = \Delta_\perp \psi$ the current density and $j_\parallel$ the current density fluctuations. The operators are the Poisson's bracket $[\alpha, \beta] = \frac{1}{r}(\partial_r \alpha \partial_\theta \beta - \partial_r \beta \partial_\theta \alpha)$, the gradient in the direction parallel to the magnetic field $\nabla_\parallel \alpha = [\psi, \alpha] - \partial_z \alpha$, the perpendicular Laplacian $\Delta_\perp \alpha = \partial_r^2 \alpha + \frac{1}{r}\partial_r \alpha + \frac{1}{r^2}\partial_\theta^2 \alpha$ and the curvature operator $G = \sin\theta \partial_r + \frac{1}{r}\cos\theta \partial_\theta$. This term is responsible for the linear couplings $m \leftarrow m \pm 1$ of modes, in particular the coupling of interchange modes which become a global ballooning eigenmode (see for example Ref. 21 and references therein). The field decomposition for any field f is $f = \sum_{m,n} f_{m,n}(r,t) \exp(i(m\theta - n\varphi))$ where $\varphi = z/R_0$ and R_0 is the major radius ; m and n denote respectively the poloidal and toroidal wave number of a mode $f_{m,n}(r,t)$. The pressure profile is fueled by a source term S_P and nonlinear relaxation phenomena are thus present in the dynamics. Boundary conditions for pressure and electric potential are flat (Neumann) on the inside boundary and fixed-value (Dirichlet) on the outside, allowing heat flux to escape the system from the outside boundary only. This model includes both current driven and ballooning (pressure driven) instabilities. Because of the presence of some small heat diffusion $\chi \Delta_\perp P$, the heat can be transported even in the absence of turbulence. In particular, when the source amplitude is low enough, this maintains the pressure gradient close to the instability threshold. Quasi steady-state or small-amplitude limit cycle behavior of the most unstable modes, or intermittent turbulence, are then observed as expected[22]. The fixed-flux nature of the model therefore allows studying the dynamics close to the instability threshold. It may be noted that the initial equilibrium does not remain an exact equilibrium of the evolution equations as the pressure profile changes. An axisymmetric perturbation therefore spontaneously develops to maintain force balance. However, this perturbation only affects $n = 0$ modes and has a slow evolution ; it is therefore of little influence on the mechanisms described in this paper.

Equations (1-3) are normalized using a magnetic shear length $L_\perp$, the Alfvén speed v_A and the Alfvén time $\tau_A = L_\perp / v_A$. The resistive parameters are $\eta = 10^{-4}$, $\nu = 3.10^{-5}$ and $\chi = 10^{-5}$. The normalized hybrid fluid Larmor radius is set to $\rho_\star^2 = 2.10^{-4}$. The free curvature parameter is $\kappa_1 = 0.5$; $\kappa_2 = \rho_\star^2 \kappa_1$ is imposed by energy conservation. We also set $\kappa_2^P = \kappa_2$. Those values are typical of edge tokamak plasmas such as JT60U, except for the resistivity, and are similar to the ones used in a previous work where cylindrical geometry and fixed gradient turbulence were considered instead[14]. The resolution is $N_x = 192$, $N_y = 192$, $N_z = 96$ and the simulation domain spans values of the safety factor $1.8 < q < 3.3$ typical of the outer part of the plasma core where both ballooning-stable and -unstable regions are expected.

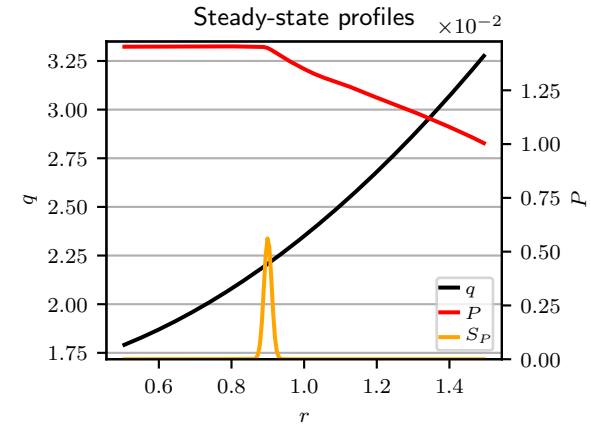

(a)

$\omega = \Delta_\perp \phi$

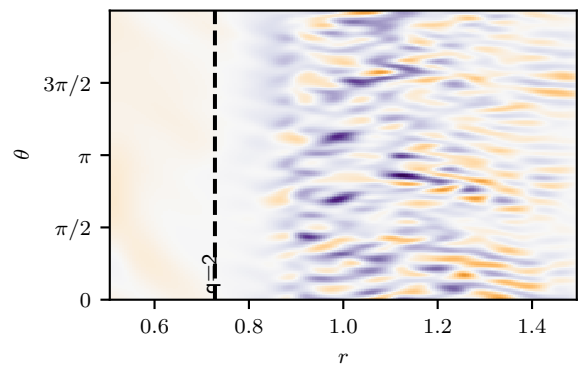

(b)

FIG. 1: (a) Profile of safety factor (black), normalized steady-state profile of pressure (red) and associated pressure source (orange). The $q = 2$ surface lies in the flat pressure region.
(b) Corresponding poloidal map of vorticity in steady-state. The $q = 2$ resonant surface is indicated by the dashed line.

By localizing the source term S_P between the low order resonant surfaces $q = 2$ and $q = 2.5$, we ensure that the system evolves towards a steady-state pressure profile that is stable (flat) in the inner zone and unstable in the outer zone, as shown on Fig. 1a. Unless otherwise noted, the heat source is a narrow radial Gaussian located at $r/a = 0.9$, corresponding to $q = q_{S_P} = 2.21$, therefore outside the $q = 2$ resonant surface. Because of the chosen Neumann boundary conditions, the radial integral of the source defines the steady-state flux injected in the system and, as long as the source is narrow enough, it is the only remaining relevant parameter. In the remainder of this paper, $S_P = 1$ will denote a source whose integral is 10^{-7} in the normalized units described above.

Since there is no other source, there is no steady-state gradient inside $r/a = 0.9$ and no small scale turbulence in this region, except for some very limited turbulence spreading. In this paper we focus on the nonlinear drive of an island with $q = 2$ helicity, located where the steady state pressure profile induced by the source is flat, see Fig. 1a. Let us emphasize that the magnetic equilibrium, as well as the initial and steady-state profiles (the latter being controlled by the source), are chosen such that the $(2, 1)$ mode is always linearly stable and is therefore not directly driven by either a classical tearing nor an interchange mode. The pressure profile is controlled by the imposed source; as can be verified in Fig. 1b, the position of the pressure source allows fine control of turbulent and stable regions in the nonlinear steady-state without any unwanted gradient induced by the turbulent heat transport. The map of vorticity shows that the turbulence develops in the edge and that neither instability nor significant fluctuations are present in the core region, Fig. 1b. It can be seen on this figure that turbulence spreading into the stable zone is present but limited to $r/a \gtrsim 0.8$, this remains true even for the highest source case considered in this work.

Neoclassical effects (bootstrap current perturbation) are not included in order to study seed island generation independently from NTM amplification[18,23,24]. Let us recall that neoclassical amplification will occur if the seeded island exceeds a critical size which depends among others on the pressure profile flattening. In our model, pressure profile perturbations therefore do not directly drive current profile perturbations. Moreover, the flat pressure profile in the core part of the simulations precludes pressure flattening around the $q = 2$ surface. This means that the islands described in the remainder of this paper are to be considered as possible seed islands for NTM generation, not as final saturated NTM islands. Moreover, the perturbation of the current profile is negligible in the simulations reported in this paper ; in particular, it has no significant effect on tearing mode growth rates.

In Fig.2 the linear growth rate of the *unstable* global ballooning modes are shown as a function of the toroidal mode number, for the asymptotic stationnary steady-state profiles corresponding to two values of the source parameter S_P. Those growth rates are computed from the mean profile in the nonlinear statistical steady-state. It shows, first that no mode $n = 1$ is unstable (note that since $q_{\min} > 1$ the mode $(m, n) = (1, 1)$ is nowhere resonant). In particular, the tearing mode $(m, n) = (2, 1)$, with rational surface $q = 2$ in the core zone, is linearly stable (very small negative growth rate, of the order of $-10^{-3}\tau_A$) for all source amplitudes, fig. 2. For all source amplitudes also, the most unstable mode is a global ballooning mode $n \simeq 7$ mainly located in the edge pressure gradient zone, thus with $m/n > q_{S_p} \approx 2.21$. In Fig. 3 (left), we show the ballooning structure of the potential for $n = 7$. We observe it is dominated by the $m \simeq 16$ mode (thus q =2.28).

The instability and transport properties of this model

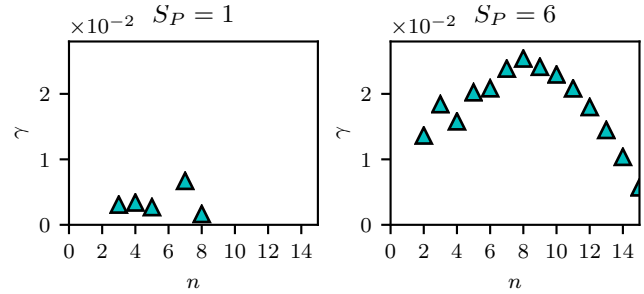

FIG. 2: Growth rates of unstable global modes, calculated from linear simulations using the steady-state pressure profiles of smallest ($S_P = 1$) and highest ($S_P = 6$) pressure source cases.

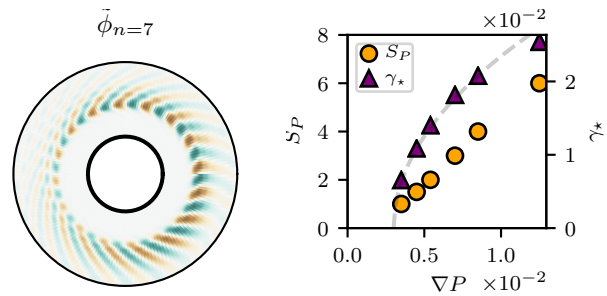

FIG. 3: Linear structure of the electric potential for the most unstable mode for the low power case $S_P = 1$ (left). Steady-state pressure source, and growth rate of the most unstable mode, as a function of the average steady-state pressure gradient (right). The dashed line is a square root fit with offset.

are shown in Fig. 3 (right). The growth rate of the most unstable mode (purple triangles) is proportional to the square root of the pressure gradient after a threshold, $\gamma \propto \sqrt{\nabla P - \nabla P_{\text{threshold}}}$ (dashed line fit), which is unsurprising for an interchange-like instability[25]. The relation between the source (corresponding to the turbulent flux) and the steady-state pressure gradient is however linear (above the threshold) ; the model exhibits limited stiffness. The tiny offset between the "source threshold" and the instability threshold corresponds to the collisional transport imposed by the diffusivity χ: below the instability threshold, there is no turbulent flux and the small pressure source feeds the diffusive flux.

III. GENERATION OF REMOTELY DRIVEN MAGNETIC ISLANDS

Here we focus on the mechanisms behind the remote generation of magnetic islands by edge turbulence. As detailed in section II, a flux-driven model including toroidal curvature is used.

The main mechanisms observed in the edge region in cylindrical fixed-gradient simulations[14] remain valid.

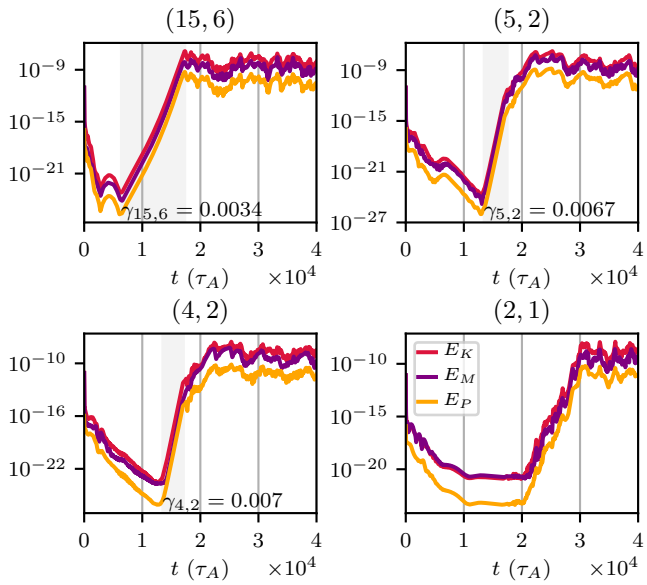

FIG. 4: Mode energy evolution of relevant modes described in Sec. III. The grey background indicates exponential growth, corresponding to either linear or quasilinear behaviour.

The generation of an island can be broken down in several phases. They are most visible in the low source case $S_P = 1$, where profile evolution is slow enough. Let us thus describe the mechanisms for this case. $E_K(m,n)$, $E_M(m,n)$ and $E_P(m,n)$ will denote respectively the kinetic (electric), magnetic and thermal energies of the mode (m,n), integrated over the whole radial domain. The time traces are shown in figure 4.

First, the pressure gradient crosses the instability threshold around $t \sim 6000\tau_A$ (see Fig. 4, top left). The most unstable mode starts growing; it is the mode $(m,n) = (15,6)$, with an average growth rate $\gamma_6 = \gamma_{15,6} = 3.4\ 10^{-3}\tau_A^{-1}$. This value is in fact somewhat lower than the result of the linear simulation with the final profile, since the profile is still slowly building up. The growth rate itself is actually slowly growing in time during this linear phase. In figure 4 (upper left) the time evolution of this mode is shown.

Second, still in the edge zone, a short quasilinear phase follows starting around $t \sim 14000\tau_A$, where nonlinear couplings drive other modes with added growth rates ; in this case, the coupling with the mode $(10,4)$ ($\gamma_{10,4} \simeq 0.003$) leads to growth of the $(5,2)$ mode with $\gamma^{\rm nl}_{5,2} = 6.7\ 10^{-3}\tau_A^{-1} \simeq \gamma_{15,6} + \gamma_{10,4}$ (figure 4, upper right). All this happens locally on (or close to) the resonant surfaces of the unstable, small-scale modes. Note that the growth of the $(5,2)$ mode on the $q = 2.5$ surface is not due to tearing instability : as shown on Fig. 2 ($S_P = 1$) the $n = 2$ mode is linearly stable ; moreover, the $(5,2)$ mode energy shown on figure 4 upper right is decreasing until the onset of the nonlinear coupling.

The overall nonlinear dynamics tends to generate multiple magnetic islands in the turbulent zone, even though the nature of the instability is interchange. What it implies with respect to mode parity deserves discussion. Indeed, it is well known that tearing-like modes are characterized by a dominant even/odd/odd parity of ψ, ϕ and P fields respectively ; the interchange parity is the opposite for all fields. However, it has been shown before that the nonlinear coupling of modes on the same resonant surface (mono-helicity situation) preserve parity, according to the following rule[6,26,27]:

- [Interchange, Interchange]→Tearing
- [Tearing, Tearing]→Tearing
- [Interchange, Tearing]→Interchange

The parity changes because the radial derivatives in the Poisson brackets invert parity. In our case, the most linearly unstable mode is a $(15,6)$ interchange-parity mode : its coupling with a $(10,4)$ interchange parity mode (linearly unstable as well) generates a $(5,2)$ tearing parity mode (island). This parity conservation mechanism is linked to the structure of the nonlinear dynamical equations, and not to the geometry of the numerical model : in particular, in a toroidal configuration, while the curvature terms linearly couple m and $m+1$ modes (changing independent interchange modes into global ballooning modes), the parity of their (m,n) components remains the same as interchange modes ; and the nonlinear coupling terms are the same as in a cylindrical configuration : the parity picture described here remains valid in toroidal geometry. In the nonlinear steady-state, a "parity cascade" saturation determines the average parity of modes[28]. One should keep in mind though, that those parity rules are only exact in a 2D mono-helicity context, where all three modes in the nonlinear coupling share the same resonant surface. However, in the 3D multi-helicity situation described here, nonlinear coupling usually occurs with modes located on different resonant surfaces. The shift between the resonant surfaces of the modes involved in the coupling breaks the parity conservation properties, and results in an overlap of interchange and tearing parities. Nevertheless, for most of the significant couplings, the distance between resonant surfaces has to be low compared to the mode radial width, and the coupling mechanism is close to the mono-helicity one. Therefore, one can expect in all cases a significant tearing-parity component in medium-scale modes, which is easily confirmed by an inspection of a Poincaré section during this phase. Conversely, the linearly unstable small-scale modes such as $(m,n) = (15,6)$ remain of mostly interchange parity at all times. At the end of this phase, the turbulent zone exhibits various islands with different helicities.

In a third phase, as can be observed in Fig. 4, due to the toroidal linear coupling, the $(5,2)$ mode drives immediately the $(4,2)$ mode, which is resonant on the $q = 2$ surface. Their mode structures are shown in Fig. 5. We observe that the (5,2) mode structure does not

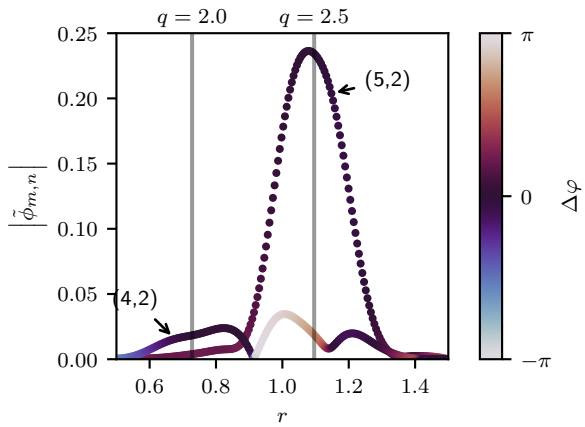

FIG. 5: Radial structure of the electric potential of the modes $(4,2)$ and $(5,2)$ during quasilinear phase ($t = 20000\tau_A$). Color indicates phase angle.

significantly cross the $q = 2$ region while the (4,2) mode structure is significant in the vicinity of both $q = 2.5$ and $q = 2$ surfaces. This indicates, first, that the $(4,2)$ mode is driven mostly on the resonant surface of the $(5,2)$ mode, in the turbulent region, and not on $q = 2$ through a radial extension of the $(5,2)$ mode. Second, as it has a broad extension which crosses the resonant $q = 2$ surface, this perturbation produces a significant island with $m = 4$ on the $q = 2$ surface. This extension comes from the fact that although the amplitude of a mode far from its resonant surface tends to be weakened by the parallel diffusion, this effect cancels at the resonance. Thus, the linear toroidal coupling, which does not exist in cylindrical cases, acts as an accelerator of the growth of the magnetic perturbations on the lowest order rational surface $q = 2$: the growth occurs immediately in the quasilinear phase while in cylindrical geometry the process is much longer because it depends on less efficient nonlinear couplings.

Finally, a nonlinear phase follows ($17000\tau_A \lesssim t \lesssim 30000\tau_A$), during which the various nonlinear mode couplings that involve less unstable modes slowly drive the low-n modes. This fills the whole spectrum, until a statistical steady-state is reached. This results on the $q = 2$ surface in an additional perturbation, mostly an $n = 1$ mode, which induces a slow growth of the island.

Unlike higher order $m/n = 2$ helical modes, it should be noted that the generation of the fundamental $(2,1)$ mode happens purely through nonlinear coupling, both, remote and resonant (local); the linear toroidal coupling from the distant $(3,1)$ mode is negligible. This has been tested in steady-state regime by first damping artificially the $(2,1)$ mode only ; when stopping the artificial damping the $(2,1)$ mode recovers as fast with $(3,1)$ mode artificially damped as with $(3,1)$ mode untouched.

The dynamics described above (early linear coupling of medium-scale modes driving harmonics on the $q = 2$ resonant surface, followed by nonlinear coupling driving the fundamental mode) differ significantly from what can be observed in comparable cylindrical simulations[14]. Indeed, in cylindrical simulations the generation of modes on the $q = 2$ surface depends only on nonlinear coupling. A 2-step process has been observed in that case as well, where in the 1st nonlinear phase a (5,2) mode extends to the $q = 2$ rational surface, and in the 2nd nonlinear phase the (2,1) mode is dominant. The absence of toroidal coupling inhibits the generation of a significant $(4,2)$ island. However it is important to stress that a (5,2) mode extension to the $q = 2$ surface can not generate a significant island either, because it is not resonant. Although a $m = 5$ separatrix would seem to appear in contour plots of the 2-dimensionnal helical flux $\chi_{q=2}$, it does not generate a 3D island structure since the perturbation of the mode averages to zero over a single poloidal turn. Indeed, inspection of Poincaré maps around $q = 2$ show that it is dominated, in the early phase, by a $m = 4$ island of negligible width.

The final steady-state of the island in toroidal and cylindrical simulations is compared in Fig.6. The average, minimum and maximum magnetic energy over the last $8000\tau_A$ of the three modes described above are shown for comparable cylindrical (left) and toroidal (center and right) simulations. By comparable we mean same q profile and similar growth rates. Although the amplitude of the $(5,2)$ mode is similar in both cases, the $(4,2)$ mode is negligible in the cylindrical simulation while it can be dominant on the $q = 2$ surface in the toroidal simulations. The significant presence of harmonics of the $(2,1)$ mode in toroidal simulations leads to a distorted island shape (Fig. 8) and complex dynamics which are described in sec. IV C. While at higher power in toroidal simulations the fundamental mode is dominant (right), the 1st harmonic is always significant in steady-state in contrast with cylindrical simulations. The high level of harmonics, in addition to bicoherence analysis of the medium-scale modes[29], might be used as an experimental signature to detect turbulence-driven magnetic islands. In particular, depending on the transport induced by such islands, the associated profile flattening may be detectable with microwave measurements such as reflectometry or electron cyclotron emission[30].

IV. $q = 2$ ISLAND DYNAMICS

A. Island size dynamics

In Fig.7 are drawn the time evolution of the island size based on the computation of the maximal radial extent of the separatrices from the helical magnetic flux

$$\chi(r) = -\int_{r_s}^{r} (1 - \frac{q}{q_s}) B_\theta dr + \sum_{m}^{m/n=q_s} \psi_{m,n}(r,t) \exp(i(m\theta - n\phi))$$

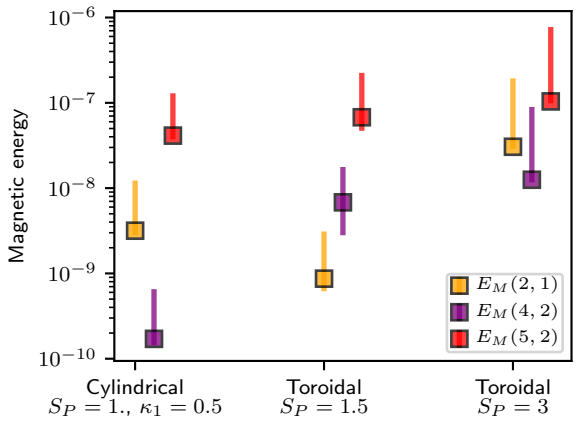

FIG. 6: Magnetic energy at saturation of the most important modes, in cylindrical and toroidal simulations.

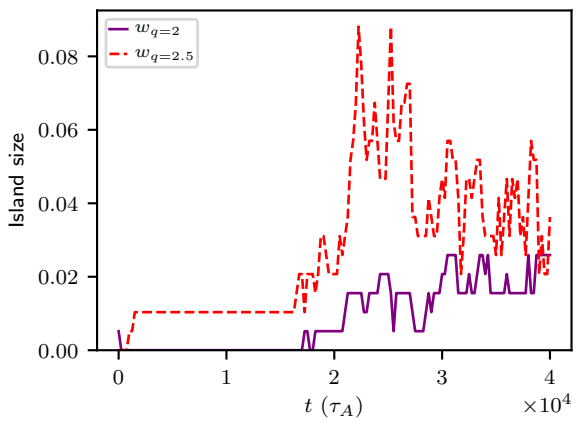

FIG. 7: Island size evolution for islands located on the $q = 2.5$ resonant surface (red dashed), and on the $q = 2$ resonant surface (solid purple)

In this graph the maximal radial extent of the islands reach up to 10% of the simulation box. They are of the same order of magnitude as the ones observed in cylindrical geometry. It can be seen however that, as in the 3D cylindrical case, the island width dynamics is much more fluctuating than in the single helicity case.

All modes of suitable parity that are resonant on a given magnetic surface contribute to the width of the magnetic island on that surface. On inspection of Fig. 7, one observes that as discussed in section III, due to the linear toroidal coupling an island appears on the $q = 2$ surface immediately after the growth of the $(5, 2)$ mode around $t \simeq 20000\tau_A$; this island is produced by the $(4, 2)$ mode. The $(2, 1)$ mode itself grows later ($t \simeq 30000\tau_A$) due to nonlinear triad interactions. In the final steady-state, the size of the islands in the turbulent edge ($q = 2.5$) and stable core zones ($q = 2$) is of the same order of magnitude, even though the magnetic energy of the $(5, 2)$ mode is much higher. Moreover, with higher pressure source level the $q = 2$ island gets comparatively stronger

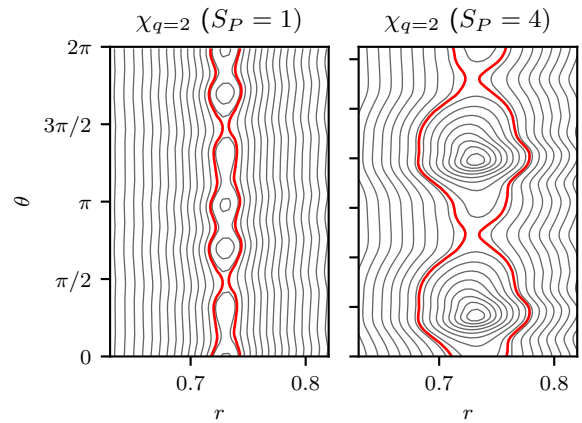

FIG. 8: Magnetic island on the $q = 2$ surface, at the end of the simulation

than the $q = 2.5$ both in terms of size and energetic content. This is discussed in Sec. IV C

B. Influence of the input power on the island size

The turbulence is the mediator tapping the free energy from the pressure gradient and driving the linearly stable $q = 2$ magnetic island. This is in contrast with the case where a current-driven instability occurs in a turbulent medium: the tearing is then unstable, and in addition to the direct nonlinear drive, the turbulence might accelerate its growth by easing reconnection through anomalous resistivity. In that latter case, turbulence is not the free energy source. Therefore, a major question concerning turbulence-generated magnetic islands is the dependence of the island size on the turbulence level. Previous work[6,14] using 2D mono-helicity and 3D cylindrical models have shown the saturated island size to be a linear function of the quasilinear anomalous heat diffusivity estimate $D_{QL} = \sum_k^{\gamma_k > 0} \frac{\gamma_k}{k_y^2}$, surprisingly not canceling in the limit of a vanishing D_{QL} (low turbulence level). On the other hand, recent work with a *linearly unstable* tearing mode have shown the presence of a finite threshold in the island size for the acceleration of island growth by turbulence[8,10] ; in other words, small islands (below some threshold) are *stabilized* by the presence of turbulence. If this result is also valid in the case of a linearly stable tearing mode, this suggests that no island would be present at all for low, but finite, turbulence levels. Therefore, the parametric dependence of the nonlinearly generated island size at low turbulence levels should be addressed. Here we use flux-driven simulations, where the steady-state heat flux corresponds to the integral of the source through energy conservation, and is thus an input parameter, as already discussed at the end of section II.

We find that the island size is proportional to the input power source (Fig. 9a). For the highest source simula-

tions, the proportionality breaks down because the island starts to be limited by the radial domain size, even though the island separatrix remains far from the domain boundary. Using the above quasilinear estimate, computed from linear simulations using (nonlinear) steady-state profiles, doesn't recover the behavior from previous works (Fig. 9b). Indeed, the island size evolution appears to be parabolic in D_{QL}. This is a consequence of the growth rate behavior of interchange-like instability being proportional to $\sqrt{\nabla P}$, the most unstable modes being the same $n \simeq 7$ for all cases, and the source (flux) being proportional to the gradient (Fig. 3, right).

The main reason for this discrepancy with previous work is that previous cylindrical simulations were run without any pressure source maintaining the initial profile (except at domain boundaries), allowing the pressure profile to relax significantly in the strongly turbulent simulations. This was checked to be not significantly altering the stability of the inner zone encompassing the $q = 2$ surface. However, the relaxed pressure profile has led to lower effective turbulence energy input through the linear terms for high flux cases than accounted for on the basis of linear simulations using the initial profile, leading to an overestimate of the turbulence level for the strong turbulence case. This is evidenced in fig. 10, using the same parameters as in work by Poyé and co-authors[14], and in particular scanning turbulence level through $\rho_\star$ instead of pressure source as well. With the addition of a pressure source maintaining the initial pressure profile, we find that the island size is indeed proportional to the turbulence level, as in toroidal simulations.

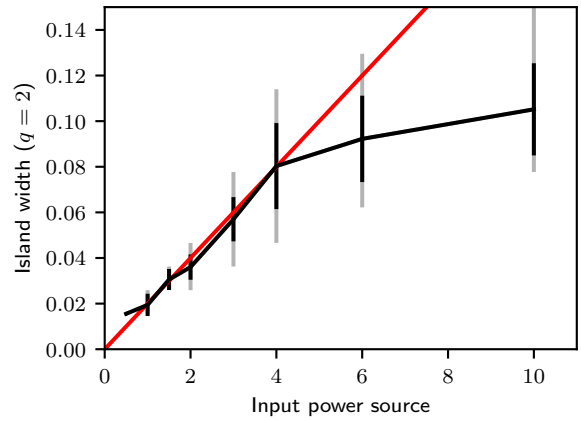

(a)

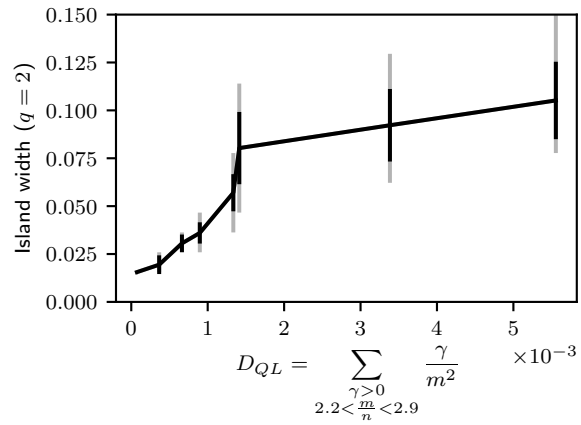

(b)

FIG. 9: Island size on $q = 2$surface, as a function of input power (a), and as a function of a quasilinear estimate of the turbulent heat diffusivity D_{QL}(b). The black errorbars correspond to the standard deviation during the last $5000\,\tau_A$ of the simulation ; the grey bars represent the min/max values.

C. Influence of the input power in the island structure

The dynamics detailed in Sec. III is observed for all values of input pressure source amplitude, albeit with slightly varying mode numbers. However, when reaching steady-state, the island is made of a superposition of various mode numbers in variable proportion. Indeed, depending on the input power (or pressure source), the dominant mode at saturation on the $q = 2$ surface decreases from $(m = 6, n = 3)$ at low pressure source to $(m = 2, n = 1)$ at high pressure source. This is readily visible in Fig. 8.

In an extreme case for simulations with a very low pressure source ($S_P \lesssim 0.5$), a limit cycle establishes where, when crossing the instability threshold, a perturbation consisting of a limited number of modes grows, flattens locally the density profile, and disappears. This perturbation is made of a single high n global mode (and its toroidal harmonics); $n = 2$ and $n = 1$ modes do not appear significantly. Therefore, the negligibly small magnetic island on the $q = 2$ surface is made of a single high n mode, generated by linear toroidal coupling.

For a slightly higher pressure source (Figure 11, $S_P = 1$), described in Sec. III, the growth of the pressure profile is fast enough that all possible modes have a non vanishing amplitude ; both the $n = 3$ and $n = 2$ perturbation dominate the nonlinear saturation regime. This produces oscillating dynamics between $n = 3$ and $n = 2$ dominance. Further increasing the pressure source ($S_P = 1.5$) leads to a $n = 2$ dominated quiescent regime, then oscillations between $n = 3$, $n = 2$ and $n = 1$ ($S_P = 2$), and $n = 1$ dominated regime ($3 < S_P < 6$). In other words, the final island is dominated by harmonics at low pressure source, and by the fundamental for higher pressure source. Intermediate values lead to oscillating regimes.

One might wonder if this dynamics is specific to the presence and nature of an underlying small scale turbulence. To answer this question, the same simulations have been run with a slightly altered safety factor profile, such that in all cases the most linearly unstable mode is the medium-scale $(7, 3)$ mode with tearing parity. Note that this mode is destabilized only if a pressure gradient is present. It is located in the outer turbulent zone;

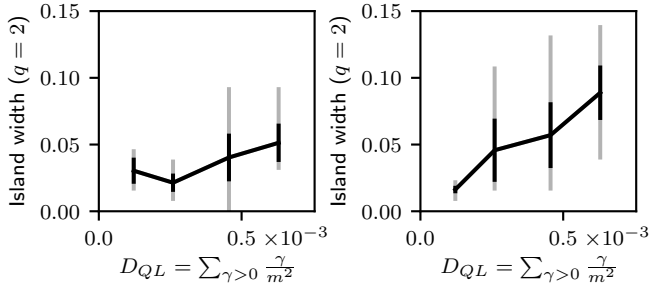

FIG. 10: Island size on $q = 2$surface, as a function of quasilinear estimate of the turbulence level, without (left) and with (right) a source maintaining the initial pressure profile. Those simulations are performed in cylindrical geometry, with parameters matching previous work[14].

the inner zone including $q = 2$ surface is still linearly stable for all modes. This altered setup allows to keep the main characteristics of the quasilinear and nonlinear phases (presence of medium-scale mode(s) of tearing parity) while offering distinct advantages. First, we can ignore the intricacies of the linear phase, such as the nature of the instability, the duration of the linear growth of various modes from initial conditions, the evolution of the pressure profile, etc. Second, it shunts the early nonlinear phase, ensuring independence from the details of the nonlinear process leading to medium-scale modes. The results, shown in Fig. 12, show more clearly the same behavior with increasing heat source: single unstable $(7, 3)$ mode linearly driving $(6, 3)$ through toroidal coupling ($S_P = 1$), oscillating regime between $n = 3$ and $n = 2$ islands ($S_P = 1.5 - 2$), quiescent $n = 2$ dominated island ($S_P = 3$), oscillations between $n = 2$ and $n = 1$ islands ($S_P = 4$), and finally $n = 1$ dominated island ($S_P = 6$).

The fact that we can recover those results without any small-scale turbulence indicates first that the direct coupling from small-scale modes is *not* a required mechanism for the remote generation of large-scale magnetic islands, and second that the coupling mechanism described here is very robust : it does not depend on the origin of the medium-scale modes.

We observe that the growing phase of the $(2, 1)$ mode is exponential (see fig. 4, bottom right) whatever the amplitude of the source. More accurately, it consists of two successive exponential phases. First, an early phase where the characteristic growth rate $\gamma^{NL}_{2,1}$ is of the order of the most unstable mode's linear growth rate $\gamma_\star$ (Fig. 13, triangles). It appears in Fig. 4 as the almost stationary phase between $10^4\tau_A < t < 2.10^4\tau_A$, and as an exponential growth for all other higher source cases. It is closer to $\gamma_\star$ for low instability cases, since in this case the second most unstable mode has a significantly lower growth rate than the most unstable mode (see fig. 2), and conversely is closer to $2\gamma_\star$ for more unstable cases. This quasilinear phase lasts until the saturation of the most

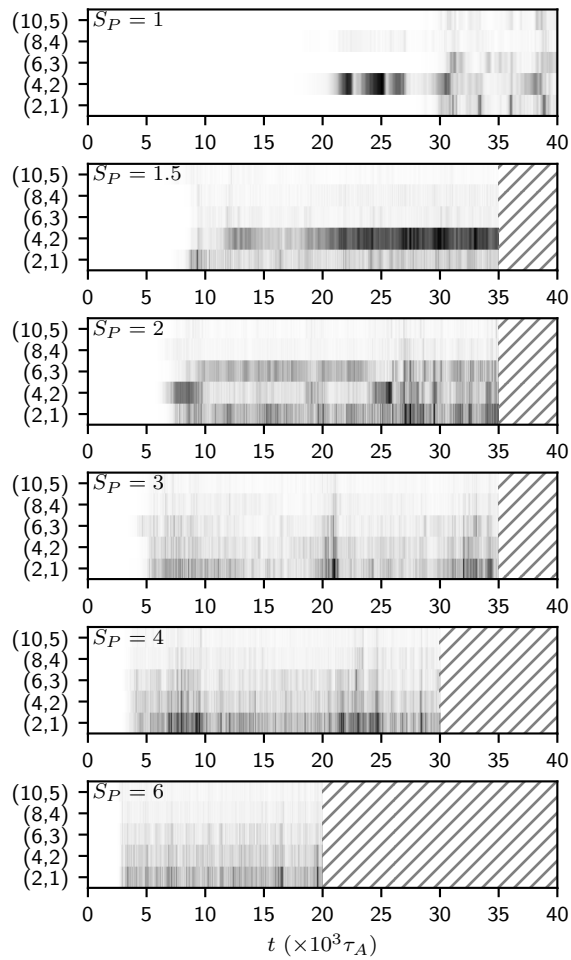

FIG. 11: Magnetic energy of modes resonant on the $q = 2$ surface, for increasing values of pressure source S_P.

unstable mode ; at this point the $(2, 1)$ mode amplitude is still very small compared its final saturation value as discussed in section III. This first phase is therefore of limited experimental relevance concerning the $(2, 1)$ mode. Then, a slower growth brings the mode to its final amplitude. This second phase exhibits significant fluctuations, due to the turbulent nature of the energy source, but still appears to be exponential ; however the associated growth rate is much lower ($\gamma^{NL} \simeq 2.9\,10^{-3}\tau_A^{-1}$ for the case discussed in Sec. III with low source $S_P = 1$; with an asymptotic value of $\gamma^{NL} \simeq 6.5\,10^{-3}\tau_A^{-1}$ for higher pressure sources) and seems approximately independent on either the source flux or the most unstable mode growth rate (Fig. 13, stars). This growth rate is also significantly faster than the inverse resistive time. The reason for this exponential behavior is unclear : since the energy for the mode growth is extracted from a steady-state gradient by an already saturated turbulence, its power is essentially constant in time; therefore, a linear or algebraic growth would be expected. While such an exponential growth driven by turbulence has been observed earlier[8],

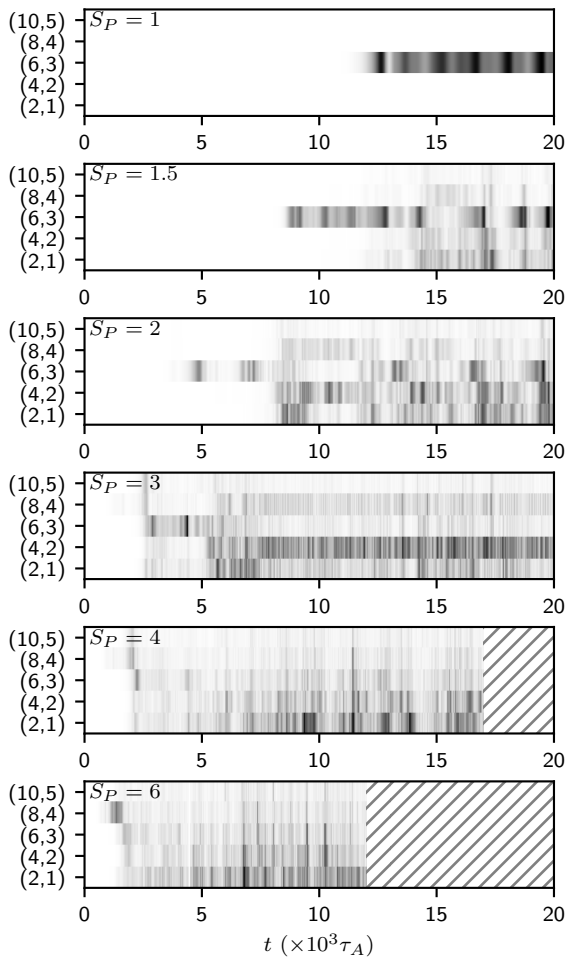

FIG. 12: Magnetic energy of modes resonant on the $q = 2$ surface, for increasing values of pressure source S_P; the most unstable mode is a tearing-like $(7, 3)$ mode.

this was before saturation of the turbulence (and for a linearly unstable mode); exponential growth was therefore unsurprising.

The duration of this second step can be much longer than the inverse linear growth rate of the underlying instability : for example, in the case described in Sec. III, for a linear growth rate of $\gamma_{15,6} = 3.4\ 10^{-3}\tau_A^{-1}$, this phase has a duration of $\sim 10^4\tau_A$. This phase is however much shorter at higher pressure source, because more modes are unstable, and the turbulent spectrum therefore reaches steady-state in less coupling steps. Moreover, the doubling of growth rates at each triad coupling leads to an explosive acceleration of the early nonlinear phase with high growth rates. Since the duration of the second phase is given by the ratio of the steady-state amplitude of the mode to the amplitude at the end of the quasilinear phase, it tends to decrease when the initial quasilinear phase is faster. A quantitative assessment of the duration of this phase is therefore difficult, since it depends on the initial conditions in addition to details of

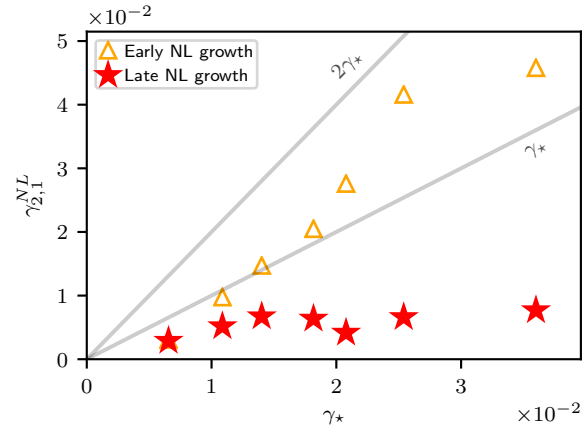

FIG. 13: Exponential growth rate of the $(2, 1)$ mode, in the fast early phase (orange triangles), and in the following slower phase (red stars)

the linear phase. A two-phase growth of $n = 1$ mode has been observed experimentally before[4,15]; however inclusion of in-situ turbulence and neoclassical effects would be mandatory for a meaningful comparison ; this is left for future work.

Let us recap the dynamics of the island on the $q = 2$ surface. Whatever the origin of the modes, the early magnetic island is a small island dominated by higher mode numbers. In the second nonlinear phase, the nonlinear couplings feed all possible modes in the system while the most unstable mode saturates; at the end of this phase the turbulent spectrum reaches a statistically steady state, and the magnetic island is dominated by its final steady-state mode number which depends on S_P (more harmonics at low power). The duration of this phase can be much longer than the inverse linear growth rate of the underlying instability ; however it is shorter for higher pressure source.

This long-term evolution could seem to be caused by profile evolution. Indeed, as the first unstable modes grow, the pressure profile continues to slowly build up and could progressively destabilize other modes ; moreover, the transport associated with the nonlinear phase leads to a complex evolution of the pressure profile before asymptotic steady-state is reached. One could therefore speculate that the dynamics presented in this paper might be a result of the linear stability evolution controlled by pressure profile changes (including nonlinear coupling to the $(m = 0, n = 0)$ mode). However, the profile evolution is not responsible for the observed dynamics. In fact, the same behavior appears after an artificial transient damping of all modes of a simulation except the $(m = 0, n = 0)$ mode ; the recovery of the turbulent spectrum, and the buildup of a magnetic island, follows the same nonlinear evolution in time as the original growth. This confirms that the dynamics presented in this paper are instead features of linear and nonlinear mode couplings.

V. CONCLUSION

We have analyzed the generation of tearing-stable magnetic islands from remote small-scale turbulence with a flux-driven 3D three-field MHD model. We find that the basic mechanisms laid out in previous works, based on the nonlinear coupling of medium-scale modes, also appear in this context, despite numerous differences in the underlying instabilities, mode couplings and transport dynamics. However, the nonlinear saturated island size is found to be proportional to the input power source, with little to no minimal size. The nonlinear generation of a magnetic island in a non-turbulent region happens in two phases. In the first phase, a small magnetic island is generated due to linear toroidal coupling from medium-scale turbulent modes. This phase is absent from cylindrical simulations. This coupling happens in the turbulent zone, far from the resonant surface. The resulting magnetic island is dominated by medium scale modes (typically n=2 to n=4 in our simulations). Then, in the 2nd phase, as the turbulent spectrum slowly evolves and reaches steady-state with respect to largest scale modes, the magnetic island grows further and ends up being dominated by a lower mode number. This second phase can take a significant time (a few orders of magnitude more than the inverse growth rate of turbulent modes) for low sources, but is significantly faster for a high-source case. This long duration makes it possibly accessible to experimental observation. The remote generation of the magnetic island in this phase happens through nonlinear mode coupling. The dominant mode number in the statistical steady-state regime decreases with increased imposed turbulent flux. Depending on the dynamics of the generation of magnetic islands in an already turbulent plasma, the evolution of the dominant mode number might be used as an experimental signature of turbulence-driven magnetic islands.

ACKNOWLEDGMENTS

The authors would like to thank Yann Camenen for fruitful discussions. This work was granted access to the HPC resources of Aix-Marseille Université financed by the project Equip@Meso (No. ANR-10-EQPX-29-01) of the program "Investissements d'Avenir" supervised by the Agence Nationale de la Recherche. It was also carried out within the framework of the EUROfusion Consortium and French Research Federation for Fusion Studies and received funding from the Euratom research and training program 2014–2018 and 2019–2020 under Grant Agreement No. 633053. The views and opinions expressed herein do not necessarily reflect those of the European Commission. Some simulations were performed with the support of EUROfusion and MARCONI-Fusion. N. D. would like to thank the referees for interesting comments and questions.

The data that support the findings of this study are available from the corresponding author upon reasonable request.

[1] S. Günter, A. Gude, M. Maraschek, S. Sesnic, Zohm, H. ASDEX Upgrade Team, and D. F. Howell. *Phys. Rev. Lett.*, 87:275001, 2001.

[2] S. Fietz, M. Maraschek, H. Zohm, L. Barrera, R. M. McDermott, M. Reich, and ASDEX Upgrade the Team. *Proceeding of the 41st EPS conference on plasma physics, Berlin*, page P2.003, 2014.

[3] A. Isayama, G. Matsunaga, Y. Hirano, and the JT-60 Team. *J. Plasma Fusion Res.*, 8:1402013, 2013.

[4] L. Bardoczi, T. L. Rhodes, A. Banon Navarro, C. Sung, T. A. Carter, R. J. La Haye, G. R. McKee, C. C. Petty, C. Chrystal, and F. Jenko. Multi-field/-scale interactions of turbulence with neoclassical tearing mode magnetic islands in the diii-d tokamak. *Physics of Plasmas*, 24(5):056106, 2017.

[5] A. Ishizawa and N. Nakajima. *Phys. Plasmas*, 17:072308, 2010.

[6] M. Muraglia, O. Agullo, S. Benkadda, M. Yagi, X. Garbet, and A. Sen. *Phys. Rev. Lett.*, 107:095003, 2011.

[7] O. Agullo, M. Muraglia, A. Poyé, S. Benkadda, M. Yagi, X. Garbet, and A. Sen. *Phys. Plasma*, 21:092303, 2014.

[8] Jiquan Li and Y. Kishimoto. Small-scale dynamo action in multiscale magnetohydrodynamic and micro-turbulence. *Physics of Plasmas*, 19(3):030705, 2012.

[9] Z.Q. Hu, Z.X. Wang, L. Wei, J.Q. Li, and Y. Kishimoto. Dual roles of shear flow in nonlinear multi-scale interactions. *Nuclear Fusion*, 56(1):016012, dec 2015.

[10] T. Liu, Z. X. Wang, Z. Q. Hu, L. Wei, J. Q. Li, and Y. Kishimoto. On the threshold of magnetic island width in nonlinear mutual destabilization of tearing mode and ion temperature gradient mode. *Physics of Plasmas*, 23(10):102508, 2016.

[11] L Wei, Z X Wang, J Q Li, Z Q Hu, and Y Kishimoto. Basic features of the multiscale interaction between tearing modes and slab ion-temperature-gradient modes. *Chinese Physics B*, 28(12):125203, dec 2019.

[12] A. Ishizawa and N. Nakajima. Thermal transport due to turbulence including magnetic fluctuation in externally heated plasma. *Nuclear Fusion*, 49(5):055015, apr 2009.

[13] W A Hornsby, P Migliano, R Buchholz, D Zarzoso, F J Casson, E Poli, and A G Peeters. On seed island generation and the nonlinear self-consistent interaction of the tearing mode with electromagnetic gyro-kinetic turbulence. *Plasma Physics and Controlled Fusion*, 57(5):054018, 2015.

[14] A. Poyé, O. Agullo, M. Muraglia, X. Garbet, S. Benkadda, A. Sen, and N. Dubuit. *Phys. Plasma*, 22:030704, 2015.

[15] L. Bardoczi, T. A. Carter, R. J. La Haye, T. L. Rhodes, and G. R. McKee. *Phys. Plasm.*, (24):122503, 2017.

[16] L Bardóczi, C Sung, A Bañón Navarro, T L Rhodes, T A Carter, and F Jenko. Interaction of magnetic islands with turbulent electron temperature fluctuations in DIII-d and in GENE nonlinear gyrokinetic simulations. *Plasma Physics and Controlled Fusion*, 62(2):025020, dec 2019.

[17] M.J. Choi, J. Kim, J.-M. Kwon, H.K. Park, Y. In, W. Lee, K.D. Lee, G.S. Yun, J. Lee, M. Kim, W.-H. Ko, J.H. Lee, Y.S. Park, Y.-S. Na, N.C. Luhmann, and B.H. Park. Multiscale interaction between a large scale magnetic island and small scale turbulence. *Nuclear Fusion*, 57(12):126058, oct 2017.

[18] M. Muraglia, O. Agullo, A. Poyé, S. Benkadda, N. Dubuit, X. Garbet, and A. Sen. Amplification of a turbulence driven seed magnetic island by bootstrap current. *Nuclear Fusion*, 57(7):072010, 2017.

[19] O. Agullo, M. Muraglia, S. Benkadda, A. Poyé, N. Dubuit, X. Garbet, and A. Sen. Nonlinear dynamics of turbulence driven magnetic islands. i. theoretical aspects. *Physics of Plasmas*, 24(4):042308, 2017.

[20] O. Agullo, M. Muraglia, S. Benkadda, A. Poyé, N. Dubuit, X. Garbet, and A. Sen. Nonlinear dynamics of turbulence driven magnetic islands. ii. numerical simulations. *Physics of Plasmas*, 24(4):042309, 2017.

[21] G. Fuhr, P. Beyer, S. Benkadda, and X. Garbet. Evidence from numerical simulations of transport-barrier relaxations in tokamak edge plasmas in the presence of electromagnetic fluctuations. *Phys. Rev. Lett.*, 101:195001, Nov 2008.

[22] F. Rath, A. G. Peeters, R. Buchholz, S. R. Grosshauser, P. Migliano, A. Weikl, and D. Strintzi. Comparison of gradient and flux driven gyro-kinetic turbulent transport. *Physics of Plasmas*, 23(5):052309, 2016.

[23] H. Reimerdes, O. Sauter, T. Goodman, and A. Pochelon. From current-driven to neoclassically driven tearing modes. *Phys. Rev. Lett.*, 88:105005, Feb 2002.

[24] J. Frank, O. Agullo, P. Maget, X. Garbet, N. Dubuit, and M. Muraglia. A reduced mhd model for itg-ntm interplay. *Physics of Plasmas*, 27(2):022119, 2020.

[25] X Garbet, P Mantica, F Ryter, G Cordey, F Imbeaux, C Sozzi, A Manini, E Asp, V Parail, R Wolf, and JET EFDA the Contributors. Profile stiffness and global confinement. *Plasma Physics and Controlled Fusion*, 46(9):1351–1373, jul 2004.

[26] M. Sato and A. Ishizawa. Nonlinear parity mixtures controlling the propagation of interchange modes. *Physics of Plasmas*, 24(8):082501, 2017.

[27] A Ishizawa, Y Kishimoto, and Y Nakamura. Multi-scale interactions between turbulence and magnetic islands and parity mixture—a review. *Plasma Physics and Controlled Fusion*, 61(5):054006, mar 2019.

[28] O. Agullo. Hdr thesis, hal archives amu collection, 2015.

[29] D. Raju, O. Sauter, and J. B. Lister. *Plasma Phys. Controlled Fusion*, 45:369, 2003.

[30] C.H.S. Amador, R. Sabot, X. Garbet, Z.O. Guimarães-Filho, and J.-H. Ahn. Determination ofqduring sawtooth from inverse evolution of BAEs in tore supra. *Nuclear Fusion*, 58(1):016010, nov 2017.